ISSN 1063-7834, Physics of the Solid State, 2018, Vol. 60, No. 11, pp. 2254–2258. © Pleiades Publishing, Ltd., 2018.
Original Russian Text © E.V. Skorokhodov, M.V. Sapozhnikov, R.V. Gorev, A.P. Volodin, V.L. Mironov, 2018, published in Fizika Tverdogo Tela, 2018, Vol. 60, No. 11, pp. 2213–2218.

MAGNETISM

Influence of the Magnetic Moment of the Probe of a Magnetic Resonance Force Microscope on the Spin-Wave Resonance Spectra

E. V. Skorokhodov[a, *], M. V. Sapozhnikov[a, b], R. V. Gorev[a], A. P. Volodin[c], and V. L. Mironov[a, b]

[a] *Institute for Physics of Microstructures, Russian Academy of Sciences, Nizhny Novgorod, 603087 Russia*
[b] *Lobachevsky State University of Nizhny Novgorod, Nizhny Novgorod, 603950 Russia*
[c] *KU Leuven, Afdeling Vaste-stoffysica en Magnetisme, 3001 Leuven, Belgium*
**e-mail: evgeny@ipmras.ru*

Received May 14, 2018

Abstract—The ferromagnetic resonance in an array of permalloy microstrips 3000 × 500 × 30 nm^3 in size, which are ordered on a rectangular 3.5 × 6 μm^2 lattice, is studied using magnetic resonance force microscopy with strong probe–sample interaction. This interaction induces intricate modifications of the observed spectra, which are manifested both in line splitting and in changes in shape. The dependences of the observed spectra on the sample–probe distance and the orientation of the magnetic moment of the probe are analyzed.

DOI: 10.1134/S1063783418110306

1. INTRODUCTION

Magnetic resonance force microscopy (MRFM) is a new high-resolution technique for studying the microwave properties of ferromagnetic nanostructures. This method, which has been developing rapidly in the recent years, is based on the detection of high-frequency oscillations of sample magnetization by a sensitive mechanical sensor in the form of a low-stiffness cantilever with a magnetic probe at the tip [1–9]. The experimental MRFM setup is shown in Fig. 1. In MRFM experiments, amplitude-modulated microwave field **h** is used to pump the sample at the resonance frequency of mechanic oscillations of the cantilever.

The basic idea behind MRFM is that the magnetic probe functions as a mechanical detector with its operating band in the kilohertz range. Under microwave pumping modulated at the natural oscillation frequency of the cantilever, the amplitude of its oscillation is proportional to the high-frequency magnetic susceptibility of the sample. This provides an opportunity to measure the ferromagnetic resonance (FMR) spectra. The MRFM technique is described in more detail below. The MRFM spectra are recorded in the form of dependences of either the amplitude or the phase of cantilever oscillations on the microwave pumping frequency or the external magnetic field. MRFM images are recorded at a constant pumping frequency by scanning the sample surface with the probe. Thus, an MRFM image represents the variation of amplitude of forced cantilever oscillations with the probe position. This variation corresponds to the amplitude distribution of magnetization oscillations at a given frequency of the microwave field. The spatial resolution of MRFM is set by the size of the region of magnetostatic sample–probe interaction and the width of the magnetic resonance line.

Owing to strong exchange interaction, the absorption of microwave radiation in ferromagnetics results in the excitation of collective magnetization oscillations (spin waves), which may be studied by MRFM. The FMR frequencies for metallic ferromagnetics lie above 0.1 GHz. Nanostructuring is an efficient technique for modifying the absorption spectrum and spatial modes of spin-wave resonances [10–12].

The results of MRFM studies of the ferromagnetic resonance in an array of permalloy microstrips in a longitudinal bias field are reported below. Since it is known that the probe may exert a considerable influence on the equilibrium magnetization distribution

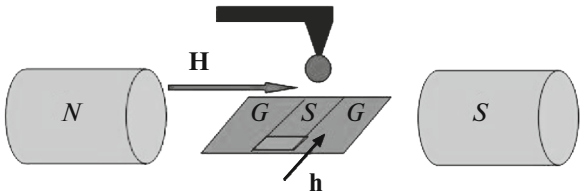

Fig. 1. Geometry of MRFM measurements.

and, consequently, the FMR spectra [13–15], specific attention was paid to this effect in the experiments.

2. MRFM EXAMINATION OF AN ARRAY OF PERMALLOY MICROSTRIPS

An FMR-array of planar permalloy $Ni_{80}Fe_{20}$ (NiFe) microstrips fabricated by lift-off lithography [16–18] was studied.

The SEM image of a part of the array is shown in Fig. 2. The strips are $3000 \times 500 \times 30$ nm^3 in size and are ordered on a rectangular lattice with periods of 6 (in the direction of the long axis) and 3.5 μm (in the transverse direction).

A magnetic resonance force microscope [19] was used in the measurements. A standard NSG-1 (NT-MDT) cantilever with a magnetic CoSm particle with a characteristic diameter of 10 μm glued to it served as the probe. The sample was positioned on a planar strip line in such a way that the magnetic component of the microwave pumping field was directed along the short axis of the strips. External bias field **H** was oriented along their long axis. The recorded MRFM spectra were room-temperature dependences of the amplitude of cantilever oscillations on the external bias field. The measurements were performed at different distances L between the magnetic probe and the sample. The pumping power was 20 dBm, and pumping frequency f was set to 5.8 GHz. The microwave field was modulated in amplitude at the resonance frequency of the cantilever. The measurements were performed in vacuum (10^{-3} Torr). The Q-factor of the probe was then 1000.

The force of sample–probe magnetic interaction, which induces cantilever oscillations, is written as

$$\mathbf{F} = -\nabla \int\limits_{V_{\text{sample}}} (\mathbf{m}\mathbf{h}_p) dV, \tag{1}$$

where **m** is the quasistatic magnetization component, which oscillates (under microwave pumping) with a frequency equal to the resonance frequency of the cantilever, and **h** is the magnetic probe field in a segment of the sample (integration is performed over sample volume V_{sample}). The z component of the force, which drives cantilever oscillations, has the following form in the case of a uniformly magnetized sample:

$$F_z = -\int\limits_{V_{\text{sample}}} \left(m_x \frac{\partial h_{px}}{\partial z} + m_y \frac{\partial h_{py}}{\partial z} + m_z \frac{\partial h_{pz}}{\partial z} \right) dV. \tag{2}$$

It can be seen that the force depends to a considerable extent on the degree of nonuniformity of the probe field in a segment of the sample. Note that the sign of this force is opposite to the sign of the magnetic-field gradient. The simplest model of the probe is a uniformly magnetized sphere with magnetic moment μ given by

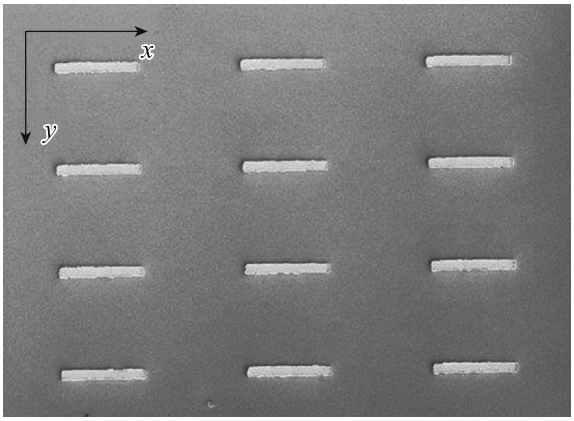

Fig. 2. SEM image of a part of the NiFe microstrip array. The strips are 3000×500 nm^2 in size.

$$\mu = \frac{4}{3}\pi R^3 M_s, \tag{3}$$

where R is the sphere radius and M_s is the saturation magnetization. This probe produces a field that corresponds to the field of a point-like magnetic dipole located at the center of the sphere:

$$\mathbf{h} = \frac{3\mathbf{r}(\mathbf{r}\boldsymbol{\mu})}{r^3} - \frac{\boldsymbol{\mu}}{r}. \tag{4}$$

Since this field is significantly nonuniform and anisotropic, the nature of interaction between the probe and the sample in MRFM depends strongly on the orientation of the magnetic moment of the probe relative to the sample magnetization.

It should be noted that the microwave field in the working gap of the microscope gives rise to the nonmagnetic sample–cantilever interaction (force $F_{\text{nonmagnetic}}$), which is induced by the potential difference between the coplanar line and the probe, Foucault currents, and the probe heating [20]. Since the microwave signal is modulated in amplitude, this interaction may also lead to the resonance cantilever oscillation build-up. Thus, the resulting force acting on the probe is the sum of magnetic and nonmagnetic forces:

$$\mathbf{F} = \mathbf{F}_{\text{nonmagnetic}} + \mathbf{F}_{\text{magnetic}}. \tag{5}$$

However, the force of magnetic interaction between the sample and the magnetic probe depends on the external field and arises only under FMR excitation, while the nonmagnetic force is constant. As a result, the FMR spectrum obtained by scanning over the external magnetic field strength has a constant background associated with the excitation of nonmagnetic cantilever oscillations [20]. If magnetic force (2) arising the FMR region is in phase with the nonmagnetic force, peaks are detected; if the magnetic and

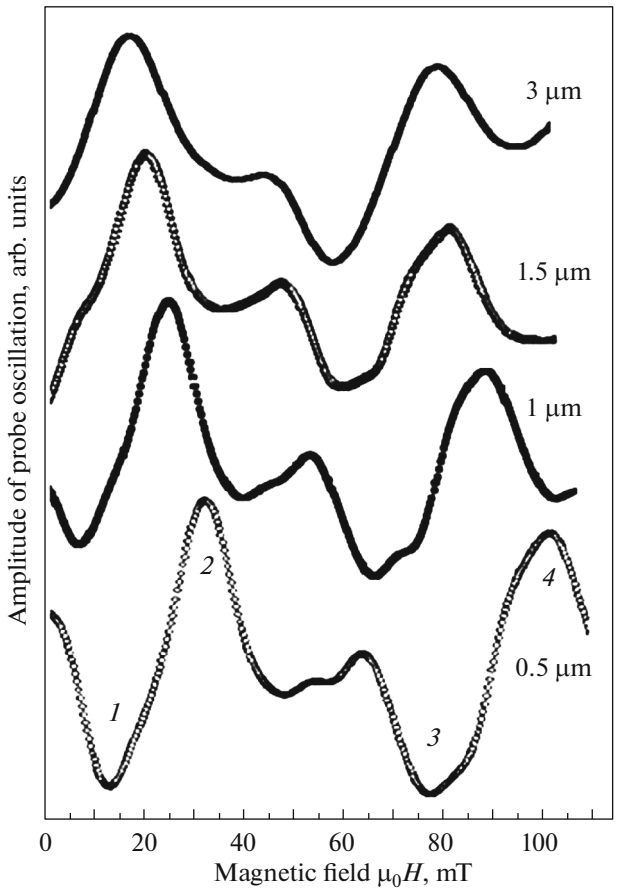

Fig. 3. MRFM spectra of FMR NiFe microstrips measured at sample–probe distances $L = 0.5$, 1, 1.5, and 3 μm with the probe magnetized perpendicularly to the sample surface. The spectra are shifted along the vertical axis for clarity. The resonances are numbered.

nonmagnetic forces are in anti-phase, dips form in the spectrum. The phase shift between the magnetic and nonmagnetic forces depends on the sign of the gradient of the probe magnetic field and changes by 180° if the gradient sign is reversed.

In the first series of experiments, the probe with its magnetic moment aligned with axis z (i.e., the normal to the sample surface) was used in MRFM measurements. The probe was positioned above the central region of one of the microstrips. The CoSm magnetic particle has large coercitivity (>2.5 T). This implies that the direction of its magnetic moment is preserved in external magnetic fields of any direction and strength used in the experiments. Figure 3 shows the MRFM spectra obtained at probe–sample distances $L = 0.5$, 1, 1.5, and 3 μm. It can be seen that the MRFM spectrum measured at $L = 0.5$ μm has two well-marked peaks at 30 and 100 mT and two dips at 10 and 80 mT.

The spectrum has a complex shape, since the bias field, which sets the FMR conditions for microstrips,

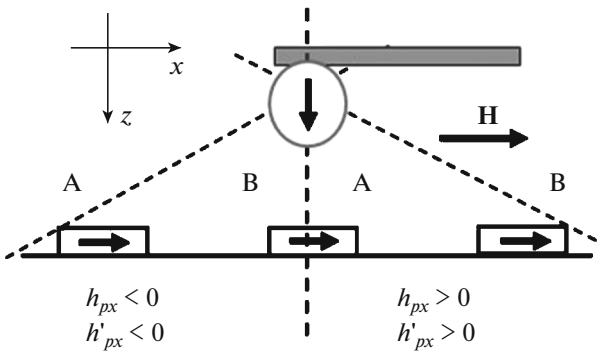

Fig. 4. Geometry of the experiment. The magnetic moment of the probe is perpendicular to the sample surface. The dashed lines represent the boundaries of conical regions with different signs of projections of the magnetic field of the probe and its gradient onto axis x.

is a combination of the external field and the magnetic probe field. Let us examine five microstrips closest to the probe (one lying directly below the probe, two microstrips positioned along the short axis, and another two along the long axis) that are likely to produce the dominant contribution to the observed spectrum. The probe field varies in strength and direction in different regions of the sample. The following three effects are essential to interpreting the shape of the spectrum: (i) since the vertical component of the probe field is transversal at any point of the sample to the shape-induced magnetic anisotropy axis of the strips, it shifts the ferromagnetic resonance toward stronger fields (see Table 1.1 in [21]); (ii) horizontal component $\mathbf{h}_{pk}$ of the probe field reduces or enhances the resonance field if this component is codirectional with the external magnetic field or directed opposite to it, respectively; (iii) since the magnetic field gradient, which sets the sign of the magnetic force, varies from one region of the sample to the other, the FMR of these regions may manifest itself as a peak or a dip in the spectrum.

Let us examine the experimental MRFM spectrum (Fig. 3). The resonances form two pairs: *1–2* and *3–4*. Each pair is a dip with a peak next to it. The weak-field dip and peak (*1–2*) include resonances resulting from the excitation of spin-wave modes. The second pair of strong-field resonances (*3–4*) corresponds to edge modes. Figure 4 provides an insight into splitting within a resonance pair. The strength and the direction of probe field $\mathbf{h}_{px}$ and the sign of field gradient $h'_{px} = \dfrac{\partial h_{px}}{\partial z}$ have different values in regions A and B. Field $\mathbf{h}_{px}$ in the strips located in region A is codirectional with the external field of the electromagnet, and its gradient is positive. Therefore, these resonances have the form of dips and are shifted toward weaker fields. The converse is true in the strips located in region B: field $\mathbf{h}_{px}$ is directed opposite to the external

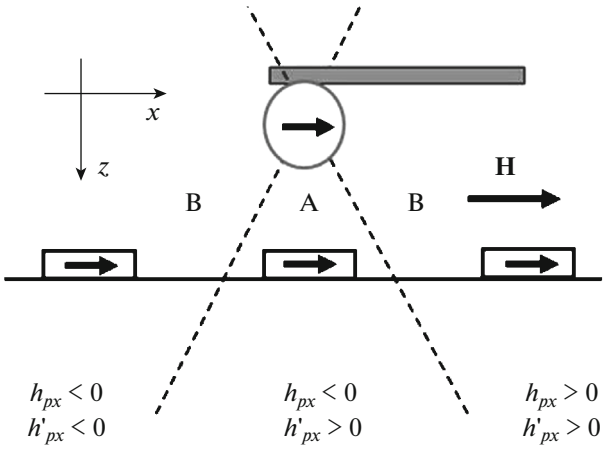

Fig. 5. Geometry of the experiment. The magnetic moment of the probe is directed along the sample surface. The dashed lines represent the boundaries of conical regions with different signs of projections of the magnetic field of the probe and its gradient onto axis *x*.

field, and its gradient is negative. This is why the resonances have the form of peaks and are shifted toward stronger fields. Thus, the difference in $\mathbf{h}_{px}$ orientation results in resonance splitting; different signs of the $\mathbf{h}_{px}$ gradient correspond to resonance peaks and dips. When the probe moves closer to the sample, $\mathbf{h}_{px}$ increases in all parts of the sample, thus shifting the spectrum as a whole toward stronger fields. The boundaries of regions A and B are determined from the following condition:

$$\frac{\partial h_{px}}{\partial z} = 0. \quad (6)$$

It follows that the relation between probe height d and coordinate x of the region boundary on the sample surface is written as

$$x = \frac{d}{\sqrt{2}}. \quad (7)$$

If the magnetic moment of the probe is directed along the sample surface (Fig. 5), the observed MRFM spectra (Fig. 6) have a distinctly different shape. This is attributed to changes in the spatial structure of the field and the field gradient produced by the magnetic probe. The space above the sample is divided in this scenario into three regions with different signs of the longitudinal component of the $\mathbf{h}_{px}$ gradient.

It can be seen from Fig. 6 that a broad dip, which corresponds to several resonance excitations near 35 and 47 mT (*1*–*3*), and a dip near 85 mT (*4*) emerge in the spectrum if the probe is located at a considerable distance (L = 3 μm) from the sample. When L decreases to 1.5 μm, the adjacent resonance excitations *1*, *2* (35 mT) and *3* (65 mT) are resolved clearly. Apparently, dips *1* and *2* in the curve for L = 3 μm correspond to resonances associated with spin-wave

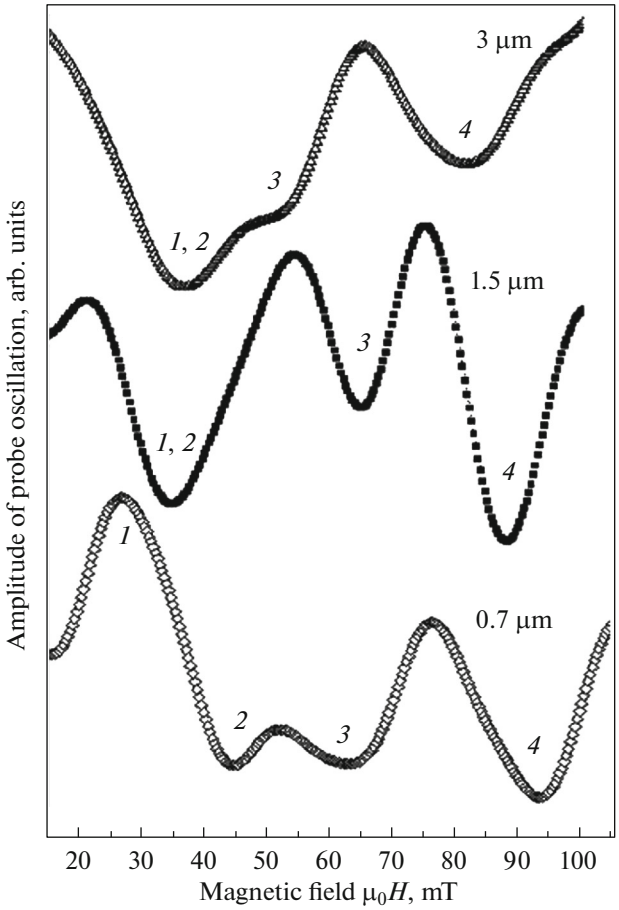

Fig. 6. MRFM spectra of FMR NiFe microstrips measured at sample–probe distances L = 0.7, 1.5, and 3 μm (from bottom to top) with the probe magnetized along the sample surface. The spectra are shifted along the vertical axis for clarity. The resonances are numbered.

oscillations, while resonances *3* and *4* are related to edge modes [16]. The variance of probe–strip distances translates into the spread of resonance magnetic fields in the array, thus broadening the dips in the experimental data. The lack of peaks is attributable to the fact that the particles producing the dominant contribution to the MRFM signal are located in region A, where the probe field gradient is positive. As L decreases further, the strips aligned with the long axis of the array (axis x in Fig. 1) enter the probe field regions with the opposite direction of the projection of the $\mathbf{h}_{px}$ field gradient (region B). As a result, the corresponding resonance (*1* in Fig. 6) is manifested as a peak at 27 mT. Height d and coordinate x of the boundary of region A on the sample surface are related in the following way in this experimental configuration:

$$x = \pm\frac{d}{2}. \quad (8)$$

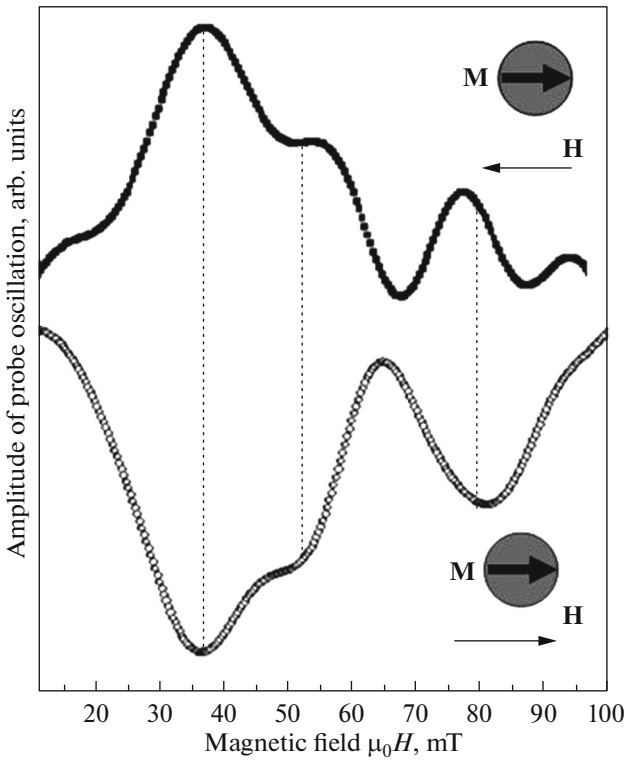

Fig. 7. MRFM spectra of FMR NiFe microstrips measured at sample–probe distance $L = 3$ μm with the probe magnetized along the sample surface. The external magnetic field is codirectional with the magnetic moment of the probe (open symbols) or is directed opposite to it (filled symbols).

Figure 7 shows the MRFM spectra obtained when the external magnetic field is codirectional with the magnetic moment of the probe and directed opposite to it. The probe is located at a distance of 3 μm and magnetized along axis *x*. When the direction of the external magnetic field is reversed, peaks change to dips, and vice versa. Such changes are in complete accord with formula (2).

3. CONCLUSIONS

The results of MRFM studies of NiFe microstrip arrays with easy-plane anisotropy were presented. Local measurement of FMR spectra was demonstrated. The dependence of MRFM spectra on the direction of the probe magnetic moment and the external magnetic field was revealed.

ACKNOWLEDGMENTS

The authors wish to thank V.A. Bykov and V.V. Polyakov for helpful advice and A.N. Reznik for his help and fruitful discussions.

This study was supported by the Russian Science Foundation, project no. 16-12-10254.

REFERENCES

1. J. A. Sidles, Appl. Phys. Lett. **58**, 2854 (1991).
2. D. Rugar, R. Budakian, H. J. Mamin, and B. W. Chui, Nature (London, U.K.) **403**, 329 (2004).
3. C. L. Degen, M. Poggio, H. J. Mamin, C. T. Rettner, and D. Rugar, Proc. Natl. Acad. Sci. U. S. A. **106**, 1313 (2009).
4. Z. Zang, P. C. Hammel, and P. E. Wigen, Appl. Phys. Lett. **68**, 2005 (1996).
5. G. De Loubens V. V. Naletov, O. Klein, J. Ben Youssef, F. Boust, and N. Vukadinovic, Phys. Rev. Lett. **98**, 127601 (2007).
6. O. Klein, G. de Loubens, V. V. Naletov, F. Boust, T. Guillet, H. Hurdequint, A. Leksikov, A. N. Slavin, V. S. Tiberkevich, and N. Vukadinovic, Phys. Rev. B **78**, 144410 (2008).
7. H.-J. Chia, F. Guo, L. M. Belova, and D. McMichael, Phys. Rev. B **86**, 184406 (2012).
8. F. Guo, L. M. Belova, and D. McMichael, Phys. Rev. Lett. **110**, 017601 (2013).
9. Yu. Obukhov, D. V. Pelekhov, J. Kim, P. Banerjee, I. Martin, E. Nazaretski, R. Movshovich, S. An, T. J. Gramila, S. Batra, and P. C. Hammel, Phys. Rev. Lett. **100**, 197601 (2008).
10. G. R. Aranda, G. N. Kakazei, J. González, and K. Y. Guslienko, J. Appl. Phys. **116**, 093908 (2014).
11. M. V. Sapozhnikov, L. I. Budarin, and E. S. Demidov, J. Magn. Magn. Mater. **449**, 68 (2018).
12. M. V. Sapozhnikov, R. V. Gorev, E. A. Karashtin, and V. L. Mironov, J. Magn. Magn. Mater. **446**, 1 (2018).
13. V. L. Mironov, A. A. Fraerman, B. A. Gribkov, O. L. Ermolaeva, A. Yu. Klimov, S. A. Gusev, I. M. Nefedov, and I. A. Shereshevskii, Phys. Met. Metallogr. **110**, 708 (2010).
14. V. L. Mironov, B. A. Gribkov, D. S. Nikitushkin, S. A. Gusev, S. V. Gaponov, A. B. Shubin, P. A. Zhdan, and C. Binns, IEEE Trans. Magn. **44**, 2296 (2008).
15. I. Lee, Yu. Obukhov, G. Xiang, A. Hauser, F. Yang, P. Banerjee, D. V. Pelekhov, and P. C. Hammel, Nature (London, U.K.) **466**, 845 (2010).
16. E. V. Skorohodov, R. V. Gorev, R. R. Yakubov, E. S. Demidov, Yu. V. Khivintsev, Yu. A. Filimonov, and V. L. Mironov, J. Magn. Magn. Mater. **424**, 118 (2017).
17. V. L. Krutyanskiy, I. A. Kolmychek, B. A. Gribkov, E. A. Karashtin, E. V. Skorohodov, and T. V. Murzina, Phys. Rev. B **88**, 094424 (2013).
18. O. G. Udalov, M. V. Sapozhnikov, A. Gribkov, E. A. Karashtin, E. V. Skorohodov, V. V. Rogov, A. Yu. Klimov, and A. A. Fraerman, Phys. Rev. B **86**, 94416 (2012).
19. E. V. Skorokhodov, M. V. Sapozhnikov, A. N. Reznik, V. V. Polyakov, V. A. Bykov, A. P. Volodin, and V. L. Mironov, Instrum. Exp. Tech. (in press).
20. Han-Jong Chia, Feng Guo, L. M. Belova, and R. D. McMichael, Phys. Rev. Lett. **108**, 087206 (2012).
21. A. G. Gurevich and G. A. Melkov, *Magnetic Oscillations and Waves* (Nauka, Moscow, 1994) [in Russian].

Translated by D. Safin